Multichannel balanced electro-optic detection for Terahertz imaging

B. Pradarutti,[1,*] **R. Müller,**[1] **G. Matthäus,**[2] **C. Brückner,**[1] **S. Riehemann,**[1] **G. Notni,**[1] **S. Nolte,**[2] **A. Tünnermann**[1,2]

[1]*Fraunhofer Institute for Applied Optics and Precision Engineering (IOF), Albert-Einstein-Str. 7, 07745 Jena, Germany*

[2]*Institute of Applied Physics, Max-Wien-Platz 1, 07743 Jena, Germany*

[*]*corresponding author: boris.pradarutti@iof.fraunhofer.de*

Abstract: We present THz imaging with 1D electro-optic sampling of ultrashort THz pulses by multichannel balanced detection. Using a lock-in technique, it combines the advantage of a high signal to noise ratio along with the fast acquisition time of multichannel detection. The object is probed by a line focus and the resolution can be adjusted. The performance of the system is demonstrated exemplarily by imaging two objects.

OCIS codes: (040.1240) Detectors: Arrays; (040.2235) Detectors: Far infrared or terahertz; (110.6795) Imaging systems: Terahertz imaging

References and links

1. D. Grischkowsky, S. Keiding, M. van Exter, and Ch. Fattinger, "Far-infrared time-domain spectroscopy with terahertz beams of dielectrics and semiconductors," J. Opt. Soc. Am. B **7**, 2006–2015 (1990).
2. G. Torosyan, C. Rau, B. Pradarutti, R. Beigang, "Generation and propagation of surface plasmons in periodic metallic structures," Appl. Phys. Lett. **85**, 3372–3374 (2004).
3. B. Pradarutti, C. Rau, G. Torosyan, R. Beigang, K. Kawase, "Plasmonic response in a one-dimensional periodic structure of metallic rods," Appl. Phys. Lett. **87**, 204105–20407 (2005).
4. K. Kawase, Y. Ogawa, Y. Watanabe, H. Inoue, "Non-destructive terahertz imaging of illicit drugs using spectral fingerprints," Opt. Express **11**, 2549–2554 (2003).
5. D. H. Auston, K. P. Cheung, P.R. Smith, "Picosecond photoconductiong Hertzian dipoles," Appl. Phys. Lett. **45**, 284–286 (1984).
6. J. Limpert, T. Schreiber, T. Clausnitzer, K. Zöllner, H.-J. Fuchs, E.-B. Kley, H. Zellmer, A. Tünnermann, "High-power femtosecond Yb-doped fiber amplifier," Opt. Express **10**, 628–638 (2002).
7. F. Röser, J. Rothhard, B. Ortac, A. Liem, O. Schmidt, T. Schreiber, J. Limpert, A. Tünnermann, "131 W 220 fs fiber laser system," Opt. Lett. **30**, 2754–2756 (2005).
8. G. Matthäus, T. Schreiber, J. Limpert, S. Nolte, G. Torosyan, R. Beigang, S. Riehemann, G. Notni, A. Tünnermann, "Surface-emitted THz generation using a compact ultrashort pulse fiber amplifier at 1060 nm," Opt. Commun. **261**, 114–117 (2006).
9. B. Pradarutti, G. Matthäus, C. Brückner, J. Limpert, S. Riehemann, G. Notni, S. Nolte, and A. Tünnermann, "Electro-optical sampling of ultrashort THz pulses by fs-laser pulses at 1060 nm," Appl. Phys. Lett. **85**, 59–62 (2006).
10. B. Pradarutti, G. Matthäus, S. Riehemann, G. Notni, S. Nolte, and A. Tünnermann, "Electro-optical sampling of ultrashort THz pulses by fs-laser pulses at 530 *nm* with $BaTiO_3$," J. Appl. Phys. **102**, 093105 (2007).
11. B. Hu, and M. C. Nuss, "Imaging with terahertz waves," Opt. Lett. **20**, 1716–1718 (1995).
12. M. L. Meade, "Lock-In Amplifier: Principles and Applications," IEEE Electrical Measurement Series 1 (Peregrinus, New York, 1983), pp. 1-45.
13. J. Xu, and X.-C. Zhang, "'Circular involute stage," Opt. Lett. **29**, 2082–2084 (2004).
14. A. Bartels, F. Hudert, C. Janke, and T. Dekorsy, "Femtosecond time-resolved optical pump-probe spectroscopy at kilohertz-scan-rates over nanosecond-time-delays without mechanical delay line", Appl. Phys. Lett. **88**, 041117 (2006).

#89303 - $15.00 USD Received 1 Nov 2007; revised 6 Dec 2007; accepted 6 Dec 2007; published 12 Dec 2007

15. A. Bartels, A. Thoma, C. Janke, T. Dekorsy, A. Dreyhaupt, S. Winnerl, and M. Helm, "High-resolution THz spectrometer with kHz scan rates," Opt. Express **14**, 430–437 (2006).
16. J. Shan, A. S. Weling, E. Knoesel, L. Bartels, M. Bonn, A. Nahata, G. A. Reider, and T. F. Heinz, "Single-shot measurement of terahertz electromagnetic pulses by use of electro-optic sampling," Opt. Lett. **25**, 426–428 (2000).
17. B. Pradarutti, G. Matthäus, S. Riehemann, G. Notni, S. Nolte, A. Tünnermann, "Advanced Analysis Concepts for Terahertz Time Domain Imaging," Opt. Commun. **279**, 248-254 (2007).
18. Q. Wu, T. D. Hewitt, X.-C. Zhang, "Two-dimensional electro-optic imaging of THz beams," Appl. Phys. Lett. **69**, 1026–1028 (1996).
19. Z. Jiang, and X.C. Zhang, "2D measurement and spatio-temporal coupling of few-cycle THz pulses," Opt. Express **5**, 243–248 (1999).
20. T. Yasuda, T. Yasui, T. Araki, E. Abraham, "Real-time two-dimensional terahertz tomography of moving objects," Opt. Commun. **267**, 128-136 (2006).
21. Z. Jiang, X. G. Xu, and X.-C. Zhang, "Improvement of terahertz imaging with a dynamic subtraction technique," Appl. Opt. **39**, 2982–2987 (2000)
22. M. Usami, R. Fukasawa, M. Tani, M. Watanabe, and K. Sakai, "Calibration free terahertz imaging based on 2D electro-optic sampling technique," Electron. Lett. **39**, 1746–1747 (2003).
23. F. Miyamaru, T.Yonera, M. Tani, and M. Hangyo, "Terahertz Two-Dimensional Electrooptic Sampling Using High Speed Complementary Metal-Oxide Semiconductor Camera", Jap. J. Appl. Phys. **43**, L489–L491 (2004).
24. W. Chan, J. Deibel, and D. Mittleman, "Imaging with terahertz radiation", Rep. Prog. Phys. **70**, 1325–1379 (2007).
25. G. Gallot and D. Grischkowsky, "Electro-optic detection of terahertz radiation," J. Opt. Soc. Am. B **16**, 1204–1212 (1999).
26. C. Brückner, S. Riehemann, G. Notni, A. Tünnermann, "Optimized THz Systems for Imaging and Spectroscopic Applications," in *2006 Joint 31st Intl. Conference on Infrared and Millimeter Waves and 14th Intl. Conference on Terahertz Electronics (IRMMW & THz)*, IEEE Proceedings 06EX1385, 36 (2006).
27. M. González and G. Santiago, V. Slezak, and A. Peuriot, "Simple synchronic detection at audio frequencies through a PC sound card", Rev. Sci. Instrum. **78**, 055108 (2007).

1. Introduction

Terahertz (THz) radiation (0.1-10 THz) has unique features making it interesting for both fundamental research [1–3] and applications e.g. in quality management, medicine, and security. While water is strongly absorptive for THz radiation, plastics, paper and foam are transparent and show distinctive contrast. From the microwave regime it is inherent that metal is nearly a perfect reflector. Also many organic substances, explosives, and drugs have characteristic absorption spectra in this frequency range [4].

On the basis of fs-lasers it is possible to generate and detect not only continuous wave (cw), but also single cycle ultrashort THz pulses covering more than one order of magnitude in the frequency range [5]. Due to the possibility of coherent detection the electric field instead of the intensity can be recorded time resolved, which makes it possible to determine the amplitude and time delay (phase) of measured pulses directly. Typically Ti:Sapphire fs-lasers at a wavelength of 800 *nm* have been used. But the size, reliability and output power restricts their field of application to laboratories. The development of modern fs-lasers like high power fiber laser amplifiers [6, 7] at a wavelength of 1060 *nm* makes it possible to build small, compact, and industrial ready THz table-top devices. Time resolved measurements at this wavelength and its frequency doubled on the basis of photoconductive switches and electro-optic sampling have already been reported [8–10].

Imaging with THz radiation has been demonstrated several times before. The easiest way is to focus the THz beam and to move the sample through the focus [11]. This method provides an excellent signal to noise ratio (SNR) by the use of phase sensitive amplification with a lock-in amplifier (LIA) [12]. However, due to the required scanning in three dimensions (two spatial and the time dimension) the scan time of this method is too long for real world applications.

In order to overcome this limitation several methods have been presented to speed up the time delay scan: The use of a fast delay stage makes it possible to acquire pixel rates up to sev-

#89303 - $15.00 USD Received 1 Nov 2007; revised 6 Dec 2007; accepted 6 Dec 2007; published 12 Dec 2007

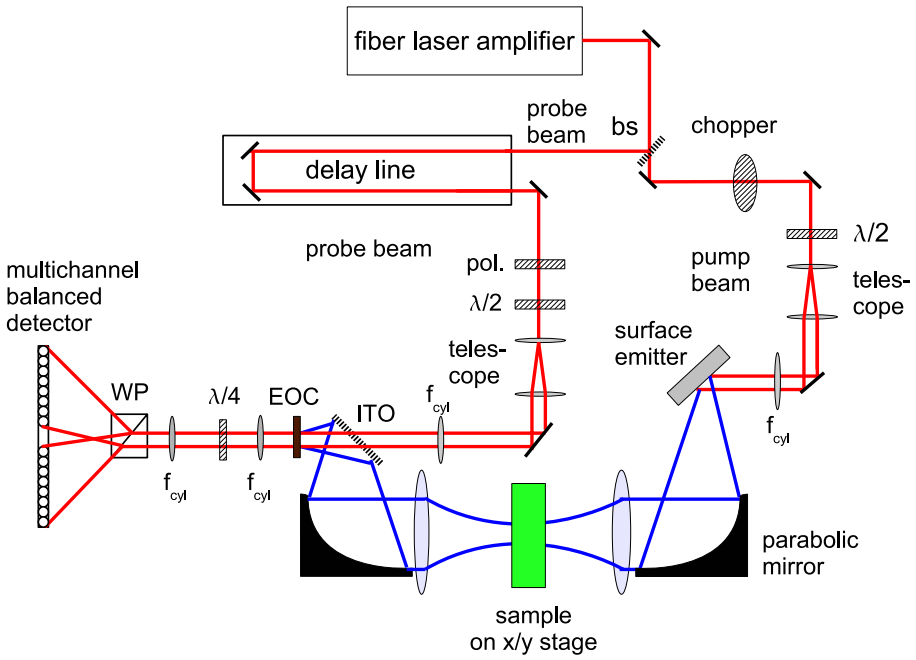

Fig. 1. Schematic setup of the THz multichannel imaging system.

eral hundred pixel per second [13]. In case of asynchronous optical sampling the mechanical delay line is replaced by two fs-lasers synchronized to two frequencies with a small difference frequency $\Delta\nu$ [14]. Data acquisition rates up to 0.25 *s* per pulse have been reported [15]. Also single shot detection [16] has been presented, but because of the lack of balanced detection the THz signal has to be extracted from a signal with high background. In addition such systems usually require expensive low repetition laser amplifier systems with high fs-pulse energies to generate sufficient THz output power. Also the time delay range is limited to several picoseconds. The use of special scanning techniques can decrease the scan time up to two orders of magnitudes, but it is limited to special materials and applications [17].

Other methods try to accelerate the spatial acquisition: 2D electro-optic sampling and 1D single shot electro-optic sampling with a CCD camera [18–20] have been demonstrated. But again the lack of balanced detection and lock-in amplifiers give need for expensive low repetition laser amplifier systems with high fs-pulse energies. Although a modulation algorithm using difference images was introduced [21–23], real lock-in techniques are not available for CCD cameras. An excellent review of different THz imaging methods can be found in [24].

In this paper we present for the first time to the best of our knowledge multichannel THz imaging with balanced electro-optic detection. Because of the balanced detection concept the THz signal can be measured without background signal and a multichannel LIA provides an additional common mode noise reduction (CMNR). This method combines all the advantages of the previously mentioned methods. It provides an excellent SNR while keeping the scan time short. This makes THz ultrashort pulse imaging applicable to real world applications.

2. Experimental setup

The ultrashort pulse THz imaging system is schematically shown in Fig. 1. It is based on a fiber amplifier laser system as described in [8], delivering up to 10 *W* at 1060 *nm*. The pulse length

#89303 - $15.00 USD Received 1 Nov 2007; revised 6 Dec 2007; accepted 6 Dec 2007; published 12 Dec 2007

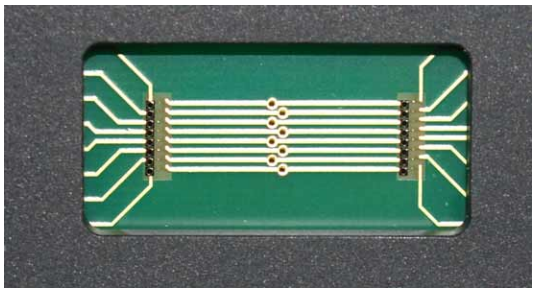

Fig. 2. 8 pixel balanced detector with InGaAs photodiodes (500 μm diameter) and 750 μm pixel pitch

is about 100 fs at a repetition rate of 75 MHz. Electro-optic sampling of ultrashort THz pulses with such a fiber amplifer system at 1060 *nm* has already been shown before [9, 10]. A detailed description of THz ultrashort pulse electro-optic sampling can be found in [25].

The electro-optic detection scheme used here has the ability to measure simultaneously 8 pixels in a line. It works with a multichannel balanced detector in combination with a multichannel LIA to increase the SNR. In order to measure a THz line, not only the detector, but also the whole THz system has to be adjusted for line scanning.

For the generation and detection of the THz pulses the fs laser pulses are split into a pump (about 96 % intensity) and probe beam (about 4 % intensity). The pump beam polarization is turned by a half wave plate to get maximum absorption (and maximum THz emission) at the emitter. The beam is expanded by a telescope and focused by a cylindrical lens to a line focus on a THz surface emitter (p-InAs). Even if the efficiency of such an emitter is smaller than the one of a photoconductive switch, it offers the advantage to form the emitted THz beam profile by adjusting the excitation laser beam profile. Therefore, the emitted THz pulses have a beam profile of a line. They are imaged by an off-axis parabolic mirror and and a lens with a demagnification of $M_f = 0.9$ to the sample. A second lens and a second off-axis parabolic mirror image the transmitted line to an electro-optic crystal (CdTe, 1 *mm* thickness) for THz detection. The complete system reproduction scale is $M = 1$.

The two metallic off-axis parabolic mirrors were made by ultraprecision turning and have a focal length of 105 mm. The aspherical lenses are made out of Zeonex ©, a material transparent for both, THz and visible light. They have a focal length of 91 *mm*. To image not only a spot but a line, the THz optics has been designed diffraction limited not only on axis but also off-axis. It was calculated using a raytracing approach in combination with physical optics algorithms to take diffraction of the THz wavelengths and the broad spectrum into account [26]. A detailed analysis of the design of this quasioptical system will be presented elsewhere.

The probe beam is guided over an optical delay line to a linear polarizer. The polarization is turned by a half wave plate to achieve maximum signal. The linear polarized probe beam is also expanded by a telescope and focused by a cylindrical lens into the detection crystal for THz probing. A second cylindrical lens collimates the beam and a quarter wave plate polarizes the probe beam elliptically. A third cylindrical lens focuses the beam again, while a Wollaston prism splits up both polarization components for the balanced detector.

The balanced detector consists of 8 balanced InGaAs photodiode pairs with 500 μm diameter and a 750 μm pixel pitch. The photodiode currents are subtracted and the difference is amplified by a factor of $5 \times 10^5\ V/A$. Thus, it is possible to measure a small signal on a high background intensity. Because the probe beam is expanded several times and only a part of the probe beam is measured by a photodiode, the fluctuations inside the beam are not negligible any longer.

#89303 - $15.00 USD Received 1 Nov 2007; revised 6 Dec 2007; accepted 6 Dec 2007; published 12 Dec 2007

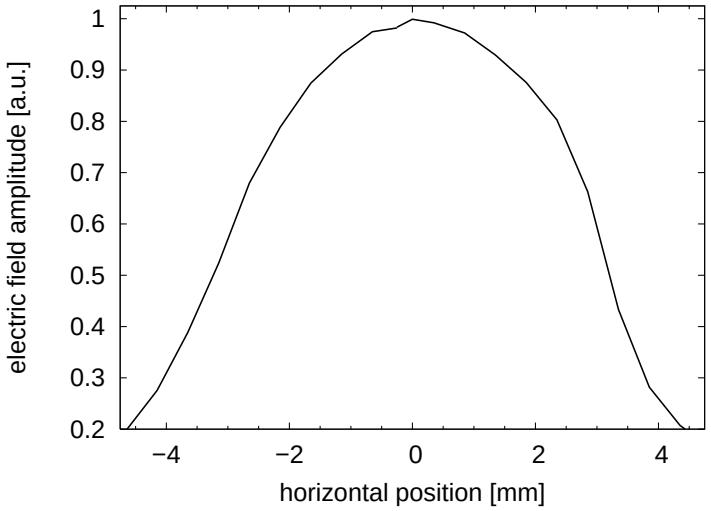

Fig. 3. Horizontal electric field amplitude distribution inside the electro-optic crystal. The FWHM is about 6.4 *mm*.

This is in opposite to a single pixel balanced detector, where the whole beam is focused onto a photodiode and the beam fluctuations are not measured. Therefore every balanced photodiode pair has been AC coupled and the amplification is bandwidth limited, representing a bandwidth filter before the amplification. Although all parts before the amplifier bring in additional noise, the suppression of the beam fluctuations increases the performance. Therefore, all balanced photodiode pairs have a common mode noise rejection (CMNR) better than 50 *dB*.

The measured signal is amplified by a LIA [12]. The LIA used provides 8 channels with a dynamic reserve better than 80 *dB*, an averaging time constant down to 2 *ms* and output filters with a slope of 12 dB/oct. While many self-made LIAs have been reported [27], systems up to 128 channels are commercially available.

The lateral resolution of the system can be tuned by the placement of a telescope between the last two cylindrical lenses or using a divergent probe beam as shown below.

For imaging the object is placed on a motorized x/y stage to move it in the focal plane. At each position 8 pulses representing 8 pixels are recorded simultaneously.

3. System characterization

The electric field distribution inside the electro-optic crystal is an image of the emitted THz radiation at the surface emitter as described in section 2. The surface emitter radiates THz pulses where it is excited by the fs laser pulses proportional to the excitation flux. So the emitted THz beam profile can be controlled by controlling the laser focus at the emitter. Even if it is less efficient than a photoconductive switch, this flexibility predestines it as a line emitter.

In the experiments the laser spot size on the emitter has been adjusted, that all balanced photodiode pairs are within the FWHM of the electric field distribution. The electric field has been probed by moving the relative position of the THz and probe beam horizontally. The maximum THz pulse amplitude is plotted in Fig. 3. The distribution has a Gaussian shape due to the Gaussian beam profile of the exciting laser. The FWHM is 6.4 *mm*.

The probe beam has been expanded more than 8 times. Only the homogeneous inner part of the Gaussian profile with less than 10 % intensity difference has been taken as probe to ensure

#89303 - $15.00 USD Received 1 Nov 2007; revised 6 Dec 2007; accepted 6 Dec 2007; published 12 Dec 2007

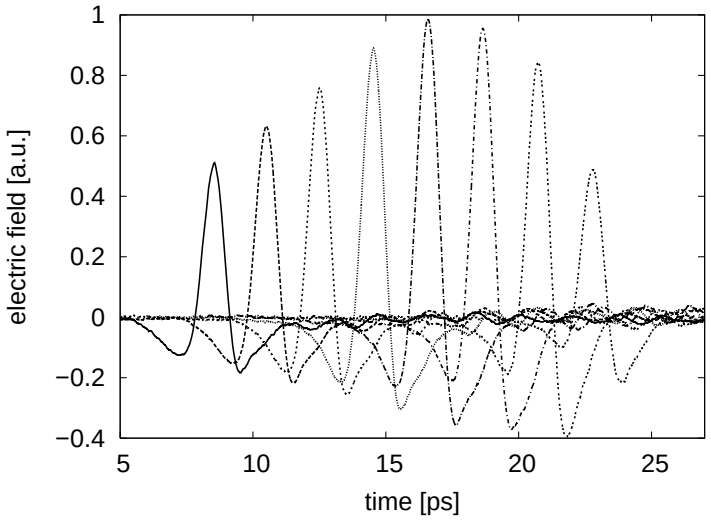

Fig. 4. Simultaneous measurement of 8 spots inside the THz electric field distribution (the electrical field traces are shifted in time for better overview). Due to the photodiode spacing and the reproduction scale, each pulse represents a horizontal lateral shift of 500 μm inside the THz focus.

that all pixels have a similar SNR. Even if this means that most of the probe laser power in the probe beam is lost, the remaining power is more than sufficient for the detection, since each photodiode needs only about 1 mW.

In the experiments 550 μm of the horizontal field distribution inside the crystal are imaged to the photodiode pitch of 750 μm at the balanced detector by using a divergent beam between the detection crystal and the balanced detector. At the detection crystal the inner part of the probe beam (about 4.5 mm) was used for probing the inner part of the THz profile shown in Fig. 3. This was confirmed by a 'knife-edge' measurement of the beam profile in the focus. It shows a THz pixel pitch of 500 μm. Taking the reproduction scale between the THz focus and the detection crystal of $M = 1.1$ into account, the settings have been confirmed well. So altogether the scan area of the line focus is about $8 \times 500\ \mu m = 4\ mm$. The FWHM for a single pixel has been determined to 0.8 mm in vertical and 1.4 mm in horizontal direction. By using different probe beam configurations the scan area and resolution could be adjusted as desired.

The 8 simultaneous measured spots are shown in Fig. 4. Each electric field trace was shifted for 2 ps in time for better overview. The envelope of the pulses shows a nearly Gaussian profile with a small asymmetry at one side.

While in this configuration most of the pump laser power is used for THz generation, the SNR of the different pixels changes by a factor of 2.

4. THz imaging

2D images have been acquired by moving the sample through the THz line focus on a metal holder. 8 spots have been measured simultaneously at each position. Although the scan time for THz imaging does not scale linearly with the number of pixels due to the lower electric field peak amplitude compared to a single pixel measurement setup, the scan time is about 5 times shorter than with a single pixel acquisition with a similar SNR.

Amplitude and time delay of the main pulse have been analyzed as described in [17]. In order to take the THz spatial beam profile into account (as visible in Fig. 4), one reference

#89303 - $15.00 USD Received 1 Nov 2007; revised 6 Dec 2007; accepted 6 Dec 2007; published 12 Dec 2007

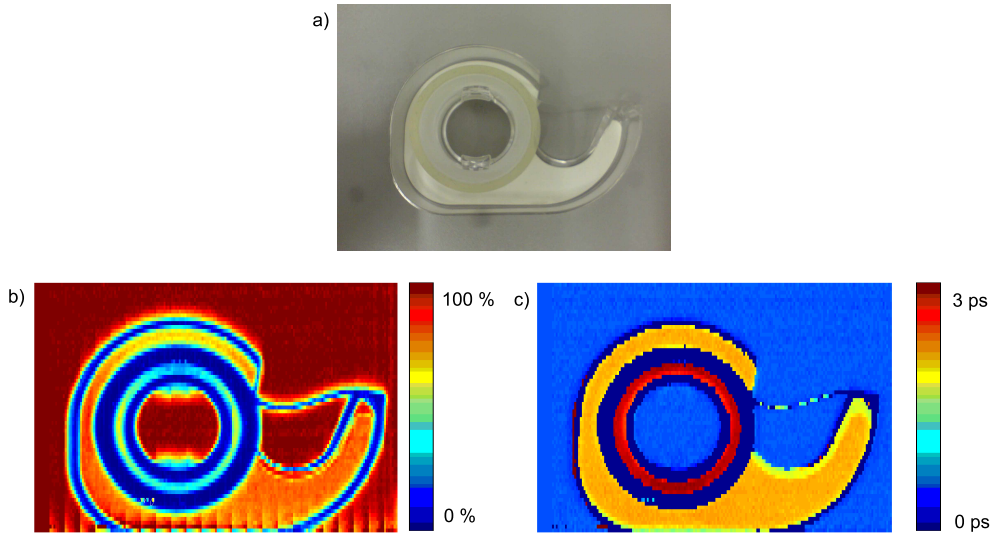

Fig. 5. Adhesive tape unwinder: a) photo; b) false color representation of THz main pulse amplitude; c) THz main pulse time delay.

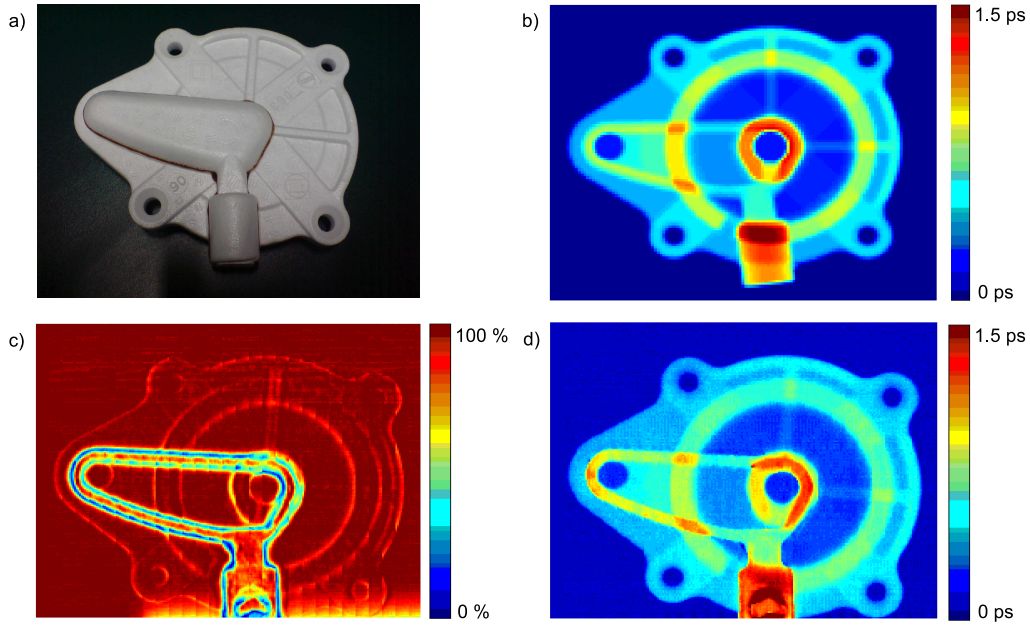

Fig. 6. Polystyrol template for iron cast: a) photo; b) optical delay calculated according to CAD data c) false color representation of THz main pulse amplitude; d) THz main pulse time delay.

#89303 - $15.00 USD Received 1 Nov 2007; revised 6 Dec 2007; accepted 6 Dec 2007; published 12 Dec 2007

measurement without a sample was taken at the beginning of each line and all the pulses/spots have been normalized to these reference values. This cancels out the different amplitudes of the different pixels and long term drifts due to laser power drifts.

The first object investigated, an adhesive tape unwinder, is shown in Fig. 5(a). It was scanned with the configuration described in section 3. We moved the sample 24×76 times and 8 electric field traces have been recorded simultaneously at each position. Altogether we measured 192×76 pixel with a pixel pitch of 500 μm in horizontal and 1000 μm in vertical direction. The scan time has been reduced from about 12 h to 2.5 h by recording 8 pixels simultaneously instead of 1 pixel. Figure 5(b) shows the false color representation of the THz main pulse amplitude. The structure of the unwinder can be sensed clearly. Even the tape, which has a lateral dimension smaller than the wavelength, can be resolved. At the bottom of the picture a band structure with a period of 8 pixels can be seen. This is due to the scattering of the metal holder used for moving the sample which introduces a crosstalk into the inhomogeneous THz distribution. Here the reference algorithm described before fails. In Fig. 5(c) the THz main pulse time delay was plotted. Only structures with dimensions of the order of the focus can be resolved as described in [17]. Because a small crosstalk between the channels does not influence the main peak time delay, no stripes are seen in this case.

Figure 6(a) shows another example, a polystyrol template for iron cast. It consists of two parts glued together. The refractive index of polystyrol for THz frequencies is about $n = 1.01$ with a negligible absorption. The sample was moved 33×240 times and again 8 electric field traces have been recorded simultaneously at each position. Altogether 264×240 pixel with a pixel pitch of 500 μm in both horizontal and vertical directions have been acquired. The false color representation of the THz main pulse amplitude is shown in Fig. 6(c). As expected only the polystyrol edges and the glue are resolved. At the edges the pulse is transmitted through a thicker and a thinner part. Due to the different time delay, the pulses are stretched in time and the amplitude is decreased accordingly. The THz pulse time delay is shown in Fig. 6(d). The picture shows all details of the polystyrol sample down to thickness differences of about 200 μm. The thickness resolution is limited by the THz pulse length, the accuracy of the delay line, and the material itself. The polystyrol consists of particles which are in the order of the wavelength. Therefore the influence of the random structure is not negligible anymore. Nevertheless the inhomogenities in the picture show time delay differences in the order of 200 fs, which is only twice the probing pulse length.

To demonstrate the performance of the system, the measurement is compared to the CAD data of the sample. The optical path differences through the sample have been computed by a raytracing program from the CAD data with a resolution of 100 μm. To take the lateral extent of the focus into account, the data has been averaged over several rays. The results are shown in Fig. 6(b). By comparing Fig. 6(b) and Fig. 6(d) all features from the CAD data are clearly resolved. Some differences like in the rounded stem are due to the glue on and inside the sample, which can also be seen in Fig. 6(c). As described above the grain structure of the measurement in Fig. 6(d) is not noise but is caused by the random particle structure inside the polystyrol.

5. Outlook

For faster scanning the number of pixels should be increased. The presented solution is scalable to more than 256 pixels in a line, so only scanning in one direction would be necessary. Therefore, a more efficient use of the laser and THz power should be achieved. Also a more homogeneous THz distribution than shown in Fig. 4 is desired to minimize the crosstalk of the channels (as visible in Fig. 5(b)). Both could be accomplished by using special beam shaping optics which produces a top hat beam profile from the Gaussian laser beam profile.

#89303 - $15.00 USD Received 1 Nov 2007; revised 6 Dec 2007; accepted 6 Dec 2007; published 12 Dec 2007

6. Conclusion

We presented THz imaging with an 8 pixel balanced detection line scanning setup. By combining each pixel with a LIA the signal to noise ratio is comparable to a single pixel detection setup, but the scan time was reduced by a factor of 5. This solution is scaleable to a complete line with more than 256 pixels and helps to bring THz imaging from experimental setups to real world applications.

Aknowlegdement

We thank Mr. Lippman and Mr. Palme (Fraunhofer IOF) for the calculation of the optical delay out of the CAD data. We thank Mr. Wöstmann and Mr. Khoja from the Fraunhofer IFAM for providing the polystyrol sample. This work was supported by the FhG internal programs under grant no. MAVO 813907.

#89303 - $15.00 USD Received 1 Nov 2007; revised 6 Dec 2007; accepted 6 Dec 2007; published 12 Dec 2007